J Sol-Gel Sci Technol (2015) 75:74–81
DOI 10.1007/s10971-015-3678-4

ORIGINAL PAPER

Effects of fluorine atoms on structure and surface properties of PANI and fluorinated PANI/GPTMS hybrid films

Qingjie Yu[1] · Jie Liu[1] · Jianming Xu[1] · Yongqiang Yin[1] · Yuanyuan Han[1] · Baoxia Li[1]

Received: 18 July 2014 / Accepted: 1 March 2015 / Published online: 25 March 2015

Abstract Fluorinated PANI/GPTMS hybrid films were successfully prepared from different polyfluoroaniline emulsions and γ-glycidoxypropyltrimethoxysilane (GPTMS) via a sol–gel method. Fluorinated PANI emulsion was generated via a chemical method in an acidic medium using 3-fluoroaniline (F_1ANI) and 3,5-bis(trifluoromethyl) aniline (F_6ANI) as monomer, respectively. The experimental results demonstrated that due to the presence of electron-withdrawing group, the introduction of fluorine atoms in polyaniline backbone can reduce the size of PANI particles and the interaction between inorganic sol and fluorinated PANI. A comparison indicated that the water repellency and thermal stability of the PF_1ANI/GPTMS hybrid films were lower than those of the PF_6ANI/GPTMS hybrid films, but its corrosion-protective ability was higher than those of the latter.

Graphical Abstract Structures of PANI (a), PF_1ANI (b), PF_6ANI (c), and PANI/GPTMS hybrids (d).

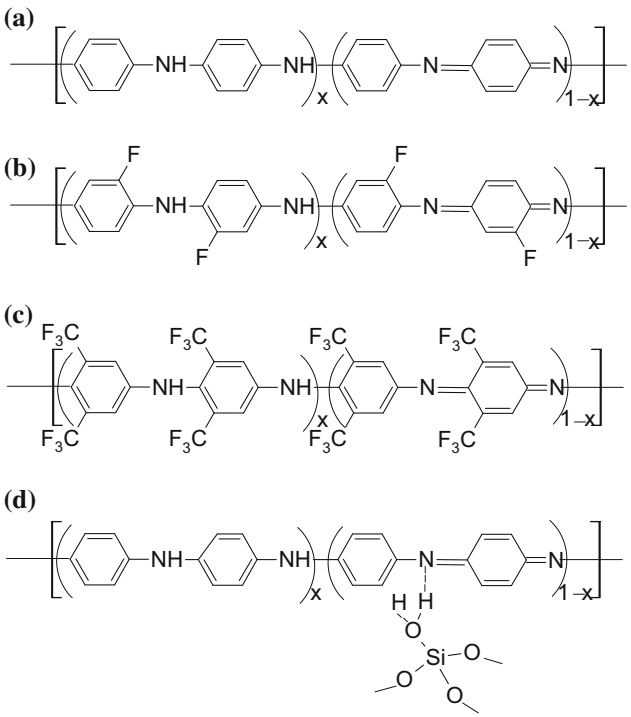

Keywords Fluorinated PANI · Fluorinated PANI/GPTMS hybrid films · Water repellency · Corrosion-protective ability

1 Introduction

Materials with a low surface free energy have recently been attracting considerable interest for water- and oil-repellent non-adhesive applications [1–3]. The reported fluorine-

✉ Qingjie Yu
qingjieyu@hqu.edu.cn

[1] School of Chemical Engineering, Huaqiao University, Xiamen 361021, People's Republic of China

containing polymers exhibit a high surface segregation of the perfluoroalkyl side chains, which causes very low free energy on their surfaces [4]. The wetting behavior is determined by the nature of the pendent chain [5, 6], the length of the pendent chain [7, 8], and the concentration of the functional surface groups [9]. Recently, considerable interest has focused on the use of hydrophobic films as protective coatings [10]. This anti-wetting property is relevant to its protection from corrosion attack. The hydrophobic coating effectively protects an underlying steel substrate from corrosion attack by preventing water from being absorbed into the coating, thus preventing the corrosive chemicals and corrosion products from diffusing through the coating [11–13].

Conducting polymers protect the metal surface by acting as a barrier and by causing anodic shift in the corrosion potential, which will cause the passivation and anodic protection of the metal substrate [14, 15]. Additionally, it has been reported that conducting polymers can reduce the corrosion rate, even after the coating has been breached and the metal surface has been exposed to the environment [16].

The corrosion-resistant properties of conducting polymers, such as polyaniline (PANI), polypyrrole, polythiophene, and poly(vinylcarbazole), on the metal substrates have been extensively studied [11, 17, 18]. In particular, PANI-SiO_2 or TiO_2 hybrid films have received extensive attention due to their potential applications in many fields, such as electrodes, electromagnetic shielding materials, corrosion-resistant coatings, sensor devices, catalysts, and others [19–25]. However, the anti-wetting property of these hybrids was found to be far from satisfactory. FANI materials have been used in polymer synthesis because of their stability and solubility [26, 27]. In addition, FANI can have a very low surface energy depending on the side-chain group. Therefore, the incorporation of FANI into siloxane-based hybrids offers tremendous potential for creating multifunctional coatings arising from the characteristic properties of FANI.

In our previous study, polyfluoroaniline/GPTMS hybrid films were directly prepared from PFANI emulsions and GPTMS through a sol–gel method [28]. In the present study, fluorinated PANI/GPTMS hybrid films were successfully prepared from different polyfluoroaniline emulsions and γ-glycidoxypropyltrimethoxysilane (GPTMS). The fluorinated PANI emulsion was generated via a chemical method in an acidic medium using 3-fluoroaniline and 3,5-bis(trifluoromethyl)aniline as monomer, respectively. The influence of the introduction of fluorine atoms in polyaniline backbone on the morphology and surface properties of PANI and fluorinated PANI/GPTMS hybrid films was investigated.

2 Experimental details

2.1 Reagents

γ-glycidoxypropyltrimethoxysilane (GPTMS, 98 %) was obtained from Nanjing UP Chemical Co., Ltd. (China). Aniline monomer (ANI, AR), 3-fluoroaniline (F_1ANI, 98 %), 3,5-bis(trifluoromethyl)aniline (F_6ANI, 98 %), sodium dodecyl sulfate (SDS, 99 %), and ammonium peroxodisulfate (APS, AR) were purchased from Sigma-Aldrich. Other chemicals, such as ethanol (ETOH, AR) and 37 % hydrochloric acid (HCl), were purchased from Sinopharm Chemical Reagent Co., Ltd. (China). All reagents were used as received without any further purification. Deionized water was used throughout the experiments.

2.2 Preparation of fluorinated PANI/GPTMS emulsions

Emulsion polymerization was performed following a typical recipe: 0.01 mol of SDS and 0.012 mol of APS were first dissolved in 20 ml of 0.5 M HCl aqueous solution in a 250 ml reaction vessel. Subsequently, 0.01mol of ANI was added to another 20 ml of 0.5 M HCl aqueous solution. The emulsion was initiated by titrating 20 ml of ANI aqueous solution into the above mixture. The polymerization was carried out with magnetic stirring at 20 °C for 24 h. PF_1ANI and PF_6ANI emulsions were formed via the same method.

2.3 Preparation of fluorinated PANI/GPTMS hybrid films

GPTMS was dissolved in the required amount of ethanol. After vigorous stirring for 1 h at 60 °C, the above PANI emulsion was added dropwise over approximately 1 h to complete the hydrolysis. The molar ratio of ANI:GPTMS was 1:10. The mixed solution was stirred for 4 h at 60 °C. Subsequently, the resultant mixture was aged in a closed container for 1 h at 25 °C and poured into polyethylene containers. PF_1ANI/GPTMS and PF_6ANI/GPTMS hybrid films were formed via the same method. Structures of PANI, PF_1ANI, PF_6ANI, and PANI/GPTMS hybrids are displayed in Fig. 1.

1060 aluminum alloy panels (Dalian Aluminum Manufacture Co., Ltd., China) were cut to 20 mm × 20 mm × 1 mm and used as substrates for coating. The samples were first cleaned with 600 mesh silicon carbide paper prior to being cleaned with 800 mesh silicon carbide paper. Subsequently, the substrates were washed with a detergent and deionized water, rinsed with acetone in an ultrasonic bath, and then dried in air.

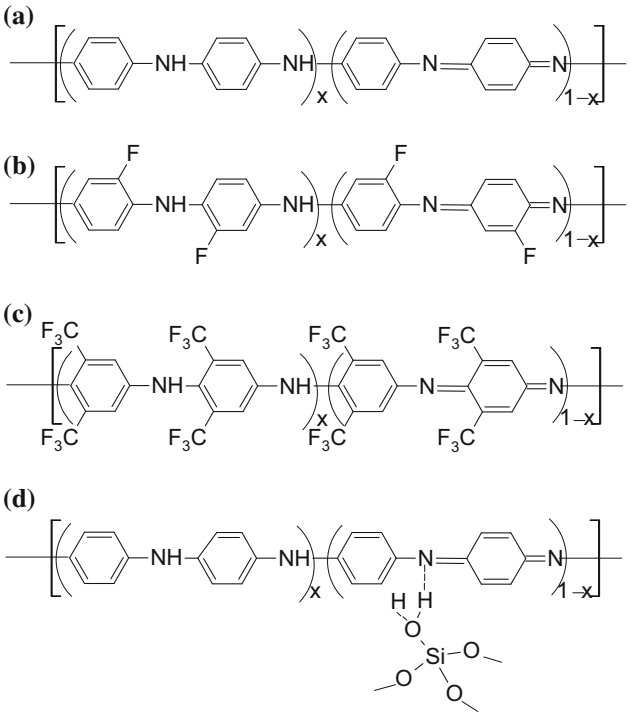

Fig. 1 Structures of PANI (**a**), PF_1ANI (**b**), PF_6ANI (**c**), and PANI/GPTMS hybrids (**d**)

The film was deposited at room temperature using a vertical dipping method with a draw speed of 10–12 cm/min. The coated film was dried in air for 30 min at 25 °C and subsequently heated to 140 °C at 0.5 °C/min in an oven under N_2.

2.4 Characterization

The chemical transformations of the hybrid gels were verified using Fourier transform infrared (FT-IR) spectroscopy (Bruker EQUINOX 55, Germany) with KBr pellets. The FT-IR spectra were recorded from 4000 to 400 cm^{-1} with a 2 cm^{-1} resolution. The surface and cross-sectional micrographs of the hybrid films were observed via scanning electron microscopy (SEM, Hitachi S-4800, Japan). Thermal degradation of the hybrid gels was carried out using thermogravimetric analysis-differential thermal analysis (TGA-DTA) calorimetry (TA Instruments SDT 2960, USA) under N_2 at a constant heating rate of 10 °C/min. The root-mean-squared roughness was measured by a three dimensional laser scanning microscope (Keyence VK-X200 K, Japan).

The contact angles of the hybrid films were measured using the sessile drop method with a contact angle meter (KRUSS DSA100, Germany) of 25 °C. The wetting liquids used for the contact angle measurements were water and methylene iodide. To avoid surface contamination, all specimens were successively washed with acetone, ethanol, and deionized water and dried prior to measurement. The static contact angle measurements were repeated with the same sample, and an average contact angle value was determined based on at least 10 measurements.

The corrosion protection capabilities of the hybrid films were assessed at an electrochemical workstation (Ametek PARSTAT 2273, USA) using potentiodynamic polarization in 0.5 mol/L aqueous sodium chloride under air. The potentiodynamic polarization was performed in a conventional electrochemical cell with a saturated calomel electrode as a reference and a titanium plate as the counter-electrode. The exposed area of the working electrode was 1.0 cm^2. All potentials were measured at 25 °C. The potential was varied from −1.5 V to positive potentials at a rate of 5 mV/s. Before the above measurements were taken, the samples were stored in a sodium chloride aqueous solution for 10 min to achieve a steady state.

3 Results and discussion

The PANI and fluorinated PANI emulsions were generated via a chemical method in an acidic medium. The prepared PANI emulsion was dark green, and no precipitation was observed in the solution after a week. The prepared PF_1ANI emulsion was reddish brown, and no precipitation was observed in the solution after a week. However, the prepared PF_6ANI emulsion was pink–white, and a small amount of flocculent precipitation and weak separation was observed in the solution after a week. Therefore, the solutions of PANI and PF_1ANI were very stable, which was very important for many practical applications.

Figure 2 displays the UV–Vis absorption spectra of PANI, PF_1ANI, and PF_6ANI emulsions. The absorption

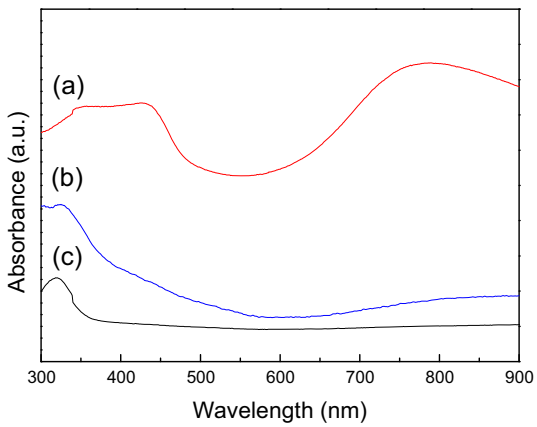

Fig. 2 UV–Vis spectra of PANI (**a**), PF_1ANI (**b**), and PF_6ANI (**c**) emulsions

peaks at 345 and 437 nm are corresponding to π–π* transition of benzenoid segments and the polaron band transition in the PANI chains, respectively. The absorption band in the range of 790–820 nm is assigned to n–π* transition for the cis-isomer of the azo linkage [23]. The π–π* transitions are in relationship with the extension of the conjugation along the polymer backbone. Comparing the absorption spectra of PF_6ANI with PANI and PFANI, this band shows a hypsochromic shift from 345 nm for PANI to 320 nm for PF_6ANI, which may be due to the presence of electron-withdrawing group in the PANI backbone, indicating a diminution in the extension of the conjugation with respect to PANI [29, 30]. The lower extension of the conjugation is the result of the dihalogenation effect, which could increase the torsion angle, therefore, decrease the overlap of molecular orbitals [29, 30].

To get more detailed insight into the effect of fluorine atoms on structure of PANI, the micrographs of PANI, PF_1ANI, and PF_6ANI particles were observed by SEM. The SEM micrographs of PANI, PF_1ANI, and PF_6ANI particles are displayed in Fig. 3. PANI rough nanospheres (Fig. 3a) are approximately 300 nm in size and present a self-aggregate. PF_1ANI rough nanospheres (Fig. 3b) are approximately 100 nm in size and highly dispersed, whereas PF_6ANI particles (Fig. 3c) are less than 40 nm and self-aggregated or spontaneously coalesced to flocculent structure. These results are consistent with the results of UV–Vis spectra.

Moreover, the introduction of fluorine atoms in polyaniline backbone has a great influence on the morphology and size distribution of PANI, PF_1ANI, and PF_6ANI particles. Due to the dihalogenation effect, the diminution in the extension of the conjugation of PF_1ANI and PF_6ANI results in the decrease of the size of PF_1ANI and PF_6ANI particles gradually. However, as for PF_6ANI, the steric hindrance and hydrophobic associating affection increase with the increase of the hydrophobic groups in the PANI backbone. The strongly hydrophobic association results in the presence of flocculent precipitation.

Figure 4 shows FT-IR spectra of PANI/GPTMS, PF_1ANI/GPTMS, and PF_6ANI/GPTMS hybrids. The peak at 3450 cm^{-1} is attributed to the N–H stretching of the aromatic amine, as well as the stretching absorption of the OH groups, and the broadband at 3150 cm^{-1} is due to the terminal quinoid N–H stretching [29, 31]. The double peak at 2931 and 2854 cm^{-1} is attributed to the aliphatic C–H stretching mode of the long alkyl tail of SDS. The absorption bands at 1640 cm^{-1} correspond to the O–H and C=N bond. The absorption peaks at 1589 and 1486 cm^{-1} are characteristic absorption peaks of PANI, which are assigned to the C=C ring stretching of the quinoid and benzenoid structure, respectively. The absorption peak at 1409 cm^{-1} is attributed to the stretch of C=C benzenoid diamine [32]. The peaks at 1310 cm^{-1} are corresponding to C–N bond. The peaks at 1045, 861, and 589 cm^{-1} are characteristic of the PANI backbone [33]. In addition to the above absorption bands originating from PANI, FT-IR

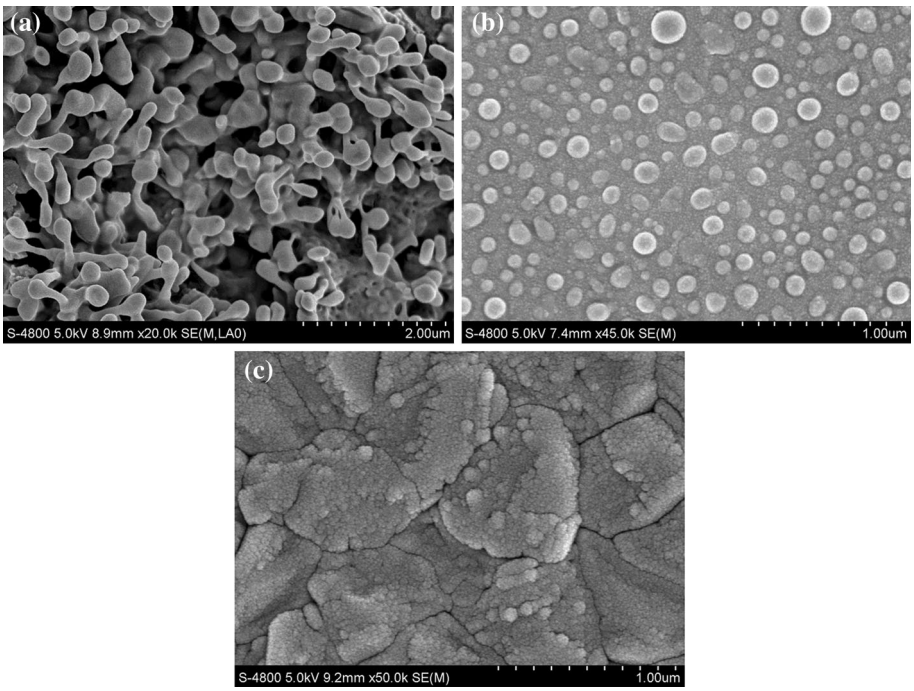

Fig. 3 SEM images of PANI (**a**), PF_1ANI (**b**), and PF_6ANI (**c**) particles

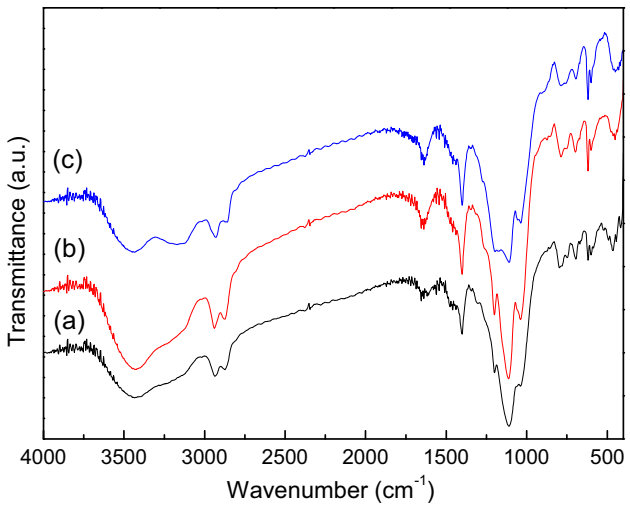

Fig. 4 FT-IR spectra of PANI/GPTMS (**a**), PF_1ANI/GPTMS (**b**), and PF_6ANI/GPTMS (**c**) hybrid gels

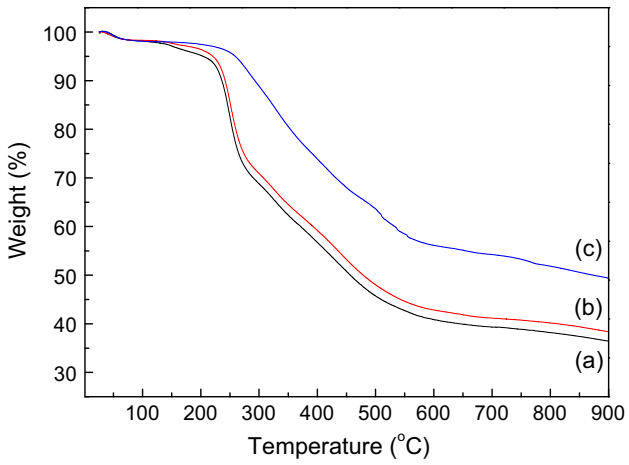

Fig. 5 TG curves of PANI/GPTMS (**a**), PF_1ANI/GPTMS (**b**), and PF_6ANI/GPTMS (**c**) hybrid gels

spectra also displayed some absorption bands that originated from siloxane monomer, including the stretching vibration absorption of the Si–O–Si groups at 1107 cm^{-1}, the Si–O stretching vibration at 800 cm^{-1}, and the Si–C stretching motion at 700 cm^{-1}.

The major difference in the FT-IR spectra of the three hybrids lies in the absorption band at approximately 1200 cm^{-1}, which is assigned to the stretching absorption of the C–F groups [9]. The presence of this peak in curve (b) and enhancement in curve (c) imply that the amount of C–F groups in PF_6ANI/GPTMS hybrids is remarkably higher than that of PF_1ANI/GPTMS hybrids, which is also consistent with the concentration of fluorine atoms calculated from stoichiometry.

Moreover, according to the sequence of curve (a), (b), and (c), a clear increase in the absorption band at 3160 cm^{-1} assigned to the N–H stretch is also observed. Silanols will be protonated at pH 1 to produce ($SiOH_2^+$) group [34, 35]. And aniline monomers in the medium will be bonded to the particles through hydrogen bonding between the amine group of aniline and the ($SiOH_2^+$) group on the surfaces of silica. The epoxy ring of GPTMS can react with water or alcohol in acidic condition to form a hydroxyl group, which tends to form hydrogen bonding with amine groups in PANI backbone [36]. However, due to the strong electronegativity of the fluorine atoms, the addition of electron-withdrawing group results in the decrease of the free electrons in PANI backbone and then the decrease of the interaction between GPTMS and PANI, which cause the increase of the N–H bond at 3160 cm^{-1}.

Figure 5 shows the thermogravimetric curves of the PANI/GPTMS, PF_1ANI/GPTMS, and PF_6ANI/GPTMS hybrid gels, respectively. The weight loss below 100 °C is assigned to the removal of water and the volatilization of solvent. The weight loss in the temperature range of 100–450 °C is mainly caused by the loss of water produced by the condensation reaction between Si and OH, the dedoping of SDS, and the decomposition of the organic components. The weight loss up to 450 °C is attributed to PFANI decomposition.

Notably, the weight loss of the PF_6ANI/GPTMS hybrids between 100 and 200 °C is less than that of the PF_1ANI/GPTMS and PANI/GPTMS hybrids. Because the weight loss at this stage is mainly attributed to the loss of absorbed water and water produced by the condensation reaction between Si and OH during the thermotreatment, the gradual decline may be relevant to the hydrophobicity of the hybrids [37]. The increased water repellency is beneficial to prevent water from being absorbed into the coating [11] and improve the thermal stability of the hybrids.

The SEM micrographs of PANI/GPTMS, PF_1ANI/GPTMS, and PF_6ANI/GPTMS hybrid films are displayed in Fig. 6. As for the PANI/GPTMS hybrids, the terminal hydroxyl group may tend to form hydrogen bonding with amine groups in the PANI backbone and make itself compatible with PANI, which is useful to prevent phase separation between inorganic sol and PANI to obtain robust and intact films. However, due to the presence of electron-withdrawing groups (fluorine) in the polymer backbone [38], the hydrogen bonding between the hydroxyl groups and amine groups will weaken in the PF_1ANI/GPTMS and PF_6ANI/GPTMS hybrids, which is prone to lead to phase separation. Furthermore, the size of the PANI, PF_1ANI, and PF_6ANI particles also strongly affects the surface morphology of the hybrid films. The small size of the particle is beneficial to obtain an uniform dispersion in the hybrids. Therefore, although the interaction between inorganic sol and PF_1ANI is weaker than that of PANI/

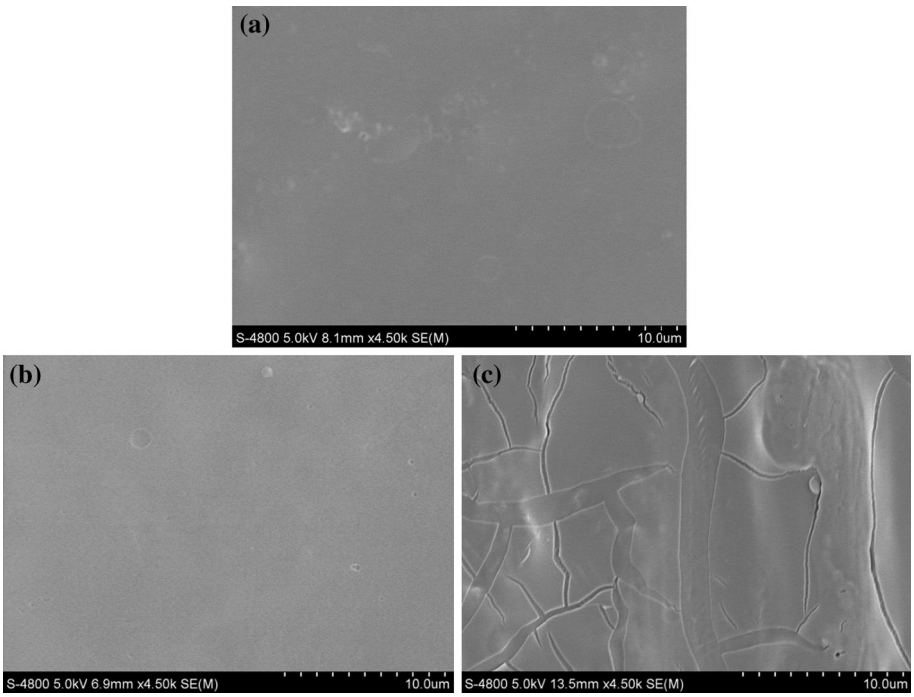

Fig. 6 SEM images of PANI/GPTMS (**a**), PF_1ANI/GPTMS (**b**), and PF_6ANI/GPTMS (**c**) hybrid films

GPTMS, the surface of the PF_1ANI/GPTMS hybrids was smoother without detectable cracks with respect to PANI/GPTMS. However, due to weak interaction and the presence of flocculent precipitation, PF_6ANI/GPTMS hybrid films were brittle and showed micro-cracks.

Table 1 lists the variations of the surface free energy of the coating films. Wettability of solid surfaces depends both on surface chemistry and on surface topography. Surface roughness is known to increase contact angles. The Ra values of the PANI/GPTMS, PF_1ANI/GPTMS, and PF_6ANI/GPTMS hybrid films obtained from three-dimensional laser scanning microscope are 0.2, 0.1, and 0.3 μm, respectively. The Ra values show that the size of the PANI, PF_1ANI, and PF_6ANI particles strongly affects the surface morphology of the hybrid films. The increase of the particle size increases the surface roughness of the hybrid films. However, as listed in Table 1, though the PF1ANI/GPTMS hybrid films possess the lowest surface roughness, it has lower surface free energy than the PANI/GPTMS hybrid films, indicated that the wetting behavior was more determined by surface chemistry in this study. The wetting behavior is determined by the nature of the pendent chain and the concentration of the functional surface groups [9]. The introduction of fluorine atoms can effectively improve water repellency of PANI/GPTMS hybrid films. Moreover, because the concentration of C–F groups in PF_6ANI is higher than that of PF_1ANI, the surface free energy of the PF_6ANI/GPTMS hybrid films is significantly lower than that of the PF_1ANI/GPTMS hybrid films. Therefore, the water repellency of the hybrid materials is governed by the hydrophobic C–F groups at the coating film–air interface, which has been confirmed by the FT-IR spectra.

The potentiodynamic polarization curves of three hybrid films are displayed in Fig. 7. The corrosion potential of the PF_1ANI/GPTMS and PANI/GPTMS hybrid films is similar; however, the corrosion current density of the former is markedly higher than that of the latter. The improved corrosion-resistant ability of the PF_1ANI/GPTMS hybrid films can be explained by their excellent water repellency and more intact films, which effectively prevented corrosion attack and improved the corrosion protection ability of the coating films [11–13].

As listed in Table 1, the PF_6ANI/GPTMS hybrid films possess excellent water repellency than the PF_1ANI/

Table 1 Contact angles and surface free energies of PANI/GPTMS, PF_1ANI/GPTMS, and PF_6ANI/GPTMS hybrid films

Monomer/GPTMS (molar ratio)	Contact angle (°)		Surface energy (mJ m^{-2})		
	H_2O	CH_2I_2	γ_s	γ_s^d	γ_s^p
PANI/GPTMS	56.6	46.8	47.19	29.26	17.93
PF_1ANI/GPTMS	104.2	81.9	16.63	15.19	1.44
PF_6ANI/GPTMS	112.1	86.1	14.30	13.81	0.49

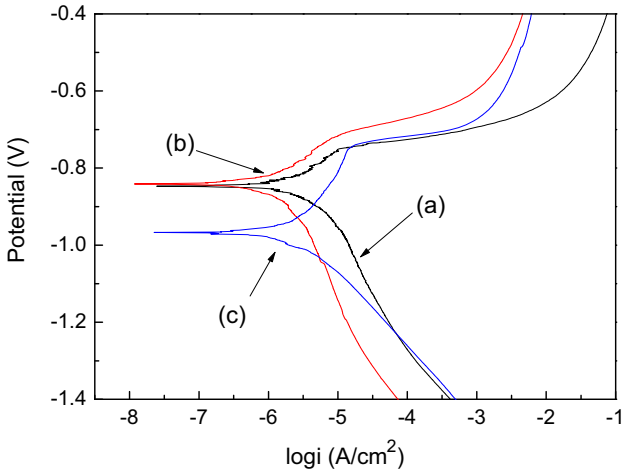

Fig. 7 Potentiodynamic polarization curves of PANI/GPTMS (**a**), PF_1ANI/GPTMS (**b**), and PF_6ANI/GPTMS (**c**) hybrid films

GPTMS hybrid films. However, the former are less able to resist corrosion compared to the latter, as indicated by a reduced corrosion potential and corrosion current density. The deterioration of the corrosion protection ability is mainly attributed to the presence of micro-cracks. The corrosive solutions more easily attack these micro-cracks to permeate into the coatings.

4 Conclusions

In this work, fluorinated PANI/GPTMS hybrid films with low surface free energy were prepared using a sol–gel process starting from fluorinated PANI emulsion and GPTMS. The experimental results revealed that the introduction of fluorine atoms in polyaniline backbone significantly influenced the morphology and surface properties of PANI and fluorinated PANI/GPTMS hybrid films. The PF_6ANI/GPTMS hybrid films exhibited excellent water repellency compared to the PANI/GPTMS and PF_1ANI/GPTMS hybrid films. Moreover, the surface of PF_1ANI/GPTMS hybrid films was homogeneous and smoother without detectable cracks compared to the PF_6ANI/GPTMS hybrid films, which would contribute to improving their corrosion-resistant capacity.

Acknowledgments The work was supported by Natural Science Foundation of Fujian Province of China (Grant No. 2011J01051) and the Fundamental Research Funds for the Central Universities (Grant No. JB-ZR1224).

References

1. Liu J, Lu X, Xin Z, Zhou CL (2013) Synthesis and surface properties of low surface free energy silane-functional polybenzoxazine films. Langmuir 29:411
2. Zhang X, Guo YG, Zhang PY, Wu ZS, Zhang ZJ (2012) Superhydrophobic and superoleophilic nanoparticle film: synthesis and reversible wettability switching behavior. ACS Appl Mater Interfaces 4:1742
3. Jung YC, Bhushan B (2009) Mechanically durable carbon nanotube-composite hierarchical structures with superhydrophobicity, self-cleaning, and low-drag. ACS Nano 3:4155
4. Urushihara Y, Nishino T (2005) Effects of film-forming conditions on surface properties and structures of diblock copolymer with perfluoroalkyl side chains. Langmuir 21:2614
5. Borkar S, Jankova K, Siesler HW, Hvilsted S (2004) New highly fluorinated styrene-based materials with low surface energy prepared by ATRP. Macromolecules 37:788
6. McHugh MA, Garach-Domech A, Park IH, Li D, Barbu E, Graham P, Tsibouklis J (2009) Impact of fluorination and side-chain length on poly(methylpropenoxyalkylsiloxane) and poly(-alkyl methacrylate) solubility in supercritical carbon dioxide. Macromolecules 35:6479
7. Sawada H, Ikeno K, Kawase T (2002) Synthesis of amphiphilic fluoroalkoxyl end-capped cooligomers containing oxime-blocked isocyanato segments: Architecture and applications of new self-assembled fluorinated molecular aggregates. Macromolecules 35:4306
8. Chang CC, Chen WC (2002) Synthesis and optical properties of polyimide-silica hybrid thin films. Chem Mater 14:4242
9. Park IJ, Lee SB, Choi CK (1997) Synthesis of fluorine-containing graft copolymers of poly (perfluoroalkylethyl methacrylate)-g-poly(methyl methacrylate) by the macromonomer technique and emulsion copolymerization method. Polymer 38:2523
10. Weng CJ, Chang CH, Peng CW, Chen SW, Yeh JM, Hsu CL, Wei Y (2011) Advanced anticorrosive coatings prepared from the mimicked xanthosoma sagittifolium-leaf-like electroactive epoxy with synergistic effects of superhydrophobicity and redox catalytic capability. Chem Mater 23:2075
11. de Leon ACC, Pernites RB, Advincula RC (2012) Superhydrophobic colloidally textured polythiophene film as superior anticorrosion coating. ACS Appl Mater Interfaces 4:3169
12. Motlagh NV, Birjandi FC, Sargolzaei J, Shahtahmassebi N (2013) Durable, superhydrophobic, superoleophobic and corrosion resistant coating on the stainless steel surface using a scalable method. Appl Surf Sci 283:636
13. Gao R, Wang J, Zhang X, Yan H, Yang W, Liu Q, Zhang M, Liu L, Takahashi K (2013) Fabrication of superhydrophobic magnesium alloy through the oxidation of hydrogen peroxide. Colloids Surf A 436:906
14. TallmanDE Spinks G, Dominis A, Wallace GC (2002) Electroactive conducting polymers for corrosion control. J Solid State Electrochem 6:73
15. Grgur BN, Krstajic NV, Vojnovic MV, Lacnjevac C, Gajic-Krstajic LJ (1998) The influence of polypyrrole films on the corrosion behavior of iron in acid sulfate solutions. Prog Org Coat 33:1
16. Reinhard G, Simon P, Rammelt U (1992) Application of electrochemical impedance spectroscopy (EIS) for characterizing the corrosion-protective performance of organic coatings on metals. Prog Org Coat 21:205
17. Kilmartin PA, Trie L, Wright GA (2002) Corrosion inhibition of polyaniline and poly (o-methoxyaniline) on stainless steels. Synth Met 131:99
18. Frau A, Pernites RB, Advincula RCA (2010) Conjugated polymer network approach to anticorrosion coatings: poly (vinylcarbazole) electrodeposition. Ind Eng Chem Res 49:9789
19. Rao AV, Latthe SS, Mahadik SA, Kappenstein C (2011) Mechanically stable and corrosion resistant superhydrophobic sol-gel coatings on copper substrate. Appl Surf Sci 257:5772

20. Kenny T, Lamare S, Aly SM, Fortin D, Brisard G, Harvey PD (2012) Reduced and oxidized forms of the Pt-organometallic version of polyaniline. Inorg Chem 51:13081
21. Shi XW, Zhang LN, Cai J, Cheng GZ, Zhang HM, Li J, Wang XH (2011) A facile construction of supramolecular complex from polyaniline and cellulose in aqueous system. Macromolecules 44:4565
22. Zou H, Wu SS, Shen J (2008) Polymer/silica nanocomposites: preparation, characterization, properties, and applications. Chem Rev 108:3893
23. Wei L, Chen Q, Gu YJ (2010) Effects of content of polyaniline doped with dodecylbenzene sulfonic acid on transparent PANI-SiO_2 hybrid conducting films. Synth Met 160:405
24. Wei L, Chen Q, Gu YJ (2010) Preparation and characterization of transparent PANI-SiO_2 hybrid conducting films. Polym Eng Sci 50:986
25. Yu QJ, Xu JM, Liu J, Li BX, Liu YJ, Han YY (2012) Synthesis and properties of PANI/SiO_2 organic-inorganic hybrid films. Appl Surf Sci 263:532
26. Ribeiro da Silva MAA, Ferreira I, Gomes JR (2007) Combined experimental and computational study of the thermochemistry of the fluoroaniline isomers. J Phys Chem B 111:2052
27. Khaled KF, Hackerman N (2004) Ortho-substituted anilines to inhibit copper corrosion in aerated 0.5 M hydrochloric acid. Electrochim Act 49:485
28. Xu JM, Yu QJ, Liu J, Yin YQ, Han YY, Li BX (2014) Preparation and characterization of polyfluoroaniline/organosiloxane hybrid films. J Sol-Gel Sci Technol 69:580
29. Cao Y, Li S, Xue Z, Guo D (1996) Spectroscopic and electrical characterization of some aniline oligomers and polyaniline. Synth Met 16:305
30. Wei Y, Focke WW, Wnek GE, Ray A, Macdiarmid AG (1989) Synthesis and electrochemistry of alkyl ring-substituted polyanilines. J Phys Chem 93:495
31. Zengin H, Erkan B (2010) Synthesis and characterization of polyaniline/silicon dioxide composites and preparation of conductive films. Polym Adv Technol 21:216
32. Cihaner A, Önal AM (2001) Synthesis and characterization of fluorine-substituted polyanilines. Eur Polym J 37:1767
33. Sharma AL, Annapoorni S, Malhotra BD (2003) Characterization of electrochemically synthesized poly (2-fluoroaniline) film and its application to glucose biosensor. Curr Appl Phys 3:239
34. Liu XX, Li YB, Bian LJ, Dou YQ, Huo YQ (2008) Electrodeposition of hybrid film of polyaniline/silica and its pseudocapacitive properties. J Solid State Electrochem 12:909
35. Curran MD, Stiegman AE (1999) Morphology and pore structure of silica xerogels made at low pH. J Non-Cryst Solids 249:62
36. Wang QG, Liu NJ, Wang XH, Li J, Zhao X, Wang F (2003) Conductive hybrids from water-borne conductive polyaniline and (3-glycidoxypropyl) trimethoxysilane. Macromolecules 36:5760
37. Kwon AH, Conklin JA, Makhinson M, Kaner RB (1997) Chemical synthesis and characterization of fluoro-substituted polyanilines. Synth Met 84:95
38. Sharma AL (2009) Electrochemical synthesis of poly (aniline-co-fluoroaniline) films and their application as humidity sensing material. Thin Solid Films 517:3350